PLANETARY TRANSIT SURVEYS

Keith Horne[1,2]

[1]Physics & Astronomy, University of St. Andrews, KY16 9SS, Scotland, UK. *(kdh1@st-and.ac.uk)*
[2]Department of Astronomy, University of Texas, Austin TX 78712, USA

Abstract

I review the status and prospects of ground-based planetary transit surveys in the era before the *Eddington* and *Kepler* missions. Over 70 extra-solar planets have been found to date by high precision radial velocity searches, but so far only one of these exhibits planetary transits. This situation should dramatically reverse in the next few years as photometric searches begin to find large numbers of "Hot Jupiters" that transit in front of their host stars.

I discuss and illustrate the methods being used to assess the planet catch of the *Eddington* mission. Scaling laws are derived to express the planet catch in terms of instrument parameters and planet type. More detailed Monte-Carlo simulations yield simulated planet catalogs. *Eddington*'s survey volume for Earth-analog planets extends to $d \approx 300$ pc, and scales with star mass, planet radius and temperature as $M^{-1/8} r^2 T$, strongly favouring large hot planets. The *Eddington* baseline design is likely to deliver only a handful of habitable Earths. The planet catch can be increased by design changes, subject of course to cost and feasibility constraints, to maximize the figure of merit $\Omega d^3 \propto \Omega (NAt)^{3/2}$, where N is the number of co-aligned telescopes, A and Ω are the effective pupil area and solid angle of each telescope, and t is the duration of the mission.

Key words: Planets: exoplanets

1. Introduction

This introduction outlines developments expected in the field of exoplanet transit surveys in the years prior to the launches of *Kepler* (2006?) and *Eddington* (2007+?). §2 then discusses analytic scaling laws, and §3 Monte-Carlo methods, developed to evaluate the planet catch of transit survey experiments.

1.1. Doppler Wobble Planets

The first "Hot Jupiter", discovered in 1995, was found by detecting Doppler wobbles of the star 51 Peg (Mayor & Queloz 1995). The star's sinusoidal radial velocity curve, with a semi-amplitude $K = 57$ m s^{-1} and period $P = 4.2$ d, implies an orbit radius $a = 0.05$ AU, planet mass $m \sin i = 0.47\ M_J$, where i is the orbit inclination, and temperature $T_{\rm eff} \sim 1400$ K.

The Doppler wobble surveys, monitoring a few thousand bright stars, have sustained for 6 years a discovery rate of about 1 planet per month. The Doppler wobble planets now number ≈ 75, with half a dozen multi-planet systems. Roughly 5% of the Sun-like stars surveyed have 'Jupiters' in the Doppler wobble detection zone ($K \gtrsim 3$ km s^{-1}, $P \lesssim 5$ yr). They spread roughly uniformly in $\log a$ and $\log m$, but are absent inside $P_{\rm min} \approx 3$ d. The mass distribution suggests that we may so far be seeing only "the tip of an iceberg", with many smaller planets lurking below the detection threshold. Longer periods are now being probed as the time baseline of the observations increases, and somewhat lower masses will be reached as the accuracy of Doppler measurements is further refined.

1.2. Planetary Transits

Transits yield information about exo-planet radii, masses, and densities. The Doppler star wobbles give $m \sin i$, a lower limit on the planet mass. If transits occur, then $\sin i \approx 1$, giving the actual planet mass m. The depth and duration of the "winks" in the transit lightcurve give i and the planet radius r.

For Jupiter transiting the Sun, since Jupiter's radius is $R_J \approx 0.1\ R_\odot$, the transit depth is $\sim 1\%$, and scales as

$$\frac{\Delta F}{F} \approx 0.01 \left(\frac{r}{R_J}\right)^2 \left(\frac{R}{R_\odot}\right)^{-2} , \qquad (1)$$

where r and R are the planet and star radii. The transit duration, for an edge-on orbit, is

$$\Delta t \approx \frac{PR}{\pi a} \approx 3 \left(\frac{P}{4\ \rm d}\right)^{1/3} \left(\frac{R}{R_\odot}\right) \left(\frac{M}{M_\odot}\right)^{-1/3} \rm h , \qquad (2)$$

where M is the star's mass. For Hot Jupiters, the 1% dimming lasting 3 hours is easy to detect with modern CCD detectors. For Earth-analog planets the depth and duration are 8×10^{-5} and 13 h respectively.

Transits occur only when the orbit is close to edge-on. For $i < 90°$, the transits become shallower and narrower, vanishing when $\cos i < (R+r)/a$. For random orientation of orbits, the probability of seeing transits is

$$P_t = \frac{R+r}{a} \approx 0.1 \left(\frac{P}{4\ \rm d}\right)^{-2/3} \left(\frac{R}{R_\odot}\right) \left(\frac{M}{M_\odot}\right)^{-1/3} . \qquad (3)$$

Proc. 1st *Eddington* workshop *"Stellar Structure and Habitable Planet Finding"*, Cordoba, 11–15 June 2001 (ESA SP-485, November 2001, F. Favata, I. W. Roxburgh & D. Galadì eds.)

For a Hot Jupiter ($P \approx 4$ d, $a \approx 0.05$ AU), the transit probability is a respectable $\approx 10\%$. For an Earth-analog ($P = 1$ yr, $a = 1$ AU) it is only 0.5%.

Secure identification of planetary transits requires verification that the depth and duration of the lightcurve "winks" repeat consistently over three or more cycles. Even when these criteria are met, a weak detection (transit depth $\approx$ lightcurve noise) can still be ambiguous. Starspots, grazing and brown dwarf eclipsing binaries, and deeply eclipsing binaries blended with foreground stars, can mimic planetary transits. Starspots have longer transits, $\Delta t \sim P/2$, and shorter lifetimes than planets. Grazing and brown dwarf eclipsing binaries with $K \gtrsim 1$ km s^{-1} may be weeded out with a couple of spectra. Background eclipsing binaries may be recognized from distinctive colour changes and/or secondary eclipses, or spatially resolved by e.g. HST imaging. Strong detections are unambiguous because the transit lightcurves have a steep ingress and egress as the planet crosses the limb, and a U-shaped minimum due to stellar limb darkening. With sufficient signal-to-noise, starspots and even moons, rings may be discovered.

1.3. HD 209458

In today's catalog of Doppler wobble planets, only one transits in front of its star. HD 209458 dims by 1.6% for 3 hours every 3.5 days (Charbonneau et al. 2000). The star is so bright (7.6 mag) that the transits were discovered with a remarkably small (10 cm!) wide-angle (6°) CCD camera (STARE). The wide field is essential for high-precision differential photometry, so that comparably bright comparison stars can be measured simultaneously.

The HD 209458 transits were quickly confirmed (e.g. Henry et al. 2000; Jha et al. 2000), most spectacularly in lightcurves captured with *HST*'s STIS spectrograph through a wide slit (Brown et al. 2001). Here the transit shape, recorded in exquisite detail, fits an immaculate limb-darkened star occulted by the planet's circular silhouette, yielding the orbit inclination $i = 86^\circ.6 \pm 0^\circ.2$ and planet radius $r = 1.35 \pm 0.06\ R_J$. The rms accuracy, better than 10^{-4}, was sufficient to place significant limits on moons ($r_{\rm moon} < 1.2\ r_\oplus$) and rings ($r_{\rm ring} < 1.8\ r_\oplus$).

Doppler wobbles revealed the planet orbiting HD 209458, and so far no new planets have been discovered by high-precision transit photometry. But this should change soon. Three search strategies are being pursued to reveal the Hot Jupiter populations of stars in globular clusters, in open clusters, and in the solar neighborhood.

1.4. Globular Clusters

First, HST's 0.1 arcsec resolution resolves main-sequence stars in the crowded cores of globular clusters. Staring for 8 days at 47 Tuc, HST monitoring of 34,000 17–21.5 mag main-sequence stars should have found 17 transits, but in fact found none (Gilliland et al. 2000). Hot Jupiter formation and/or survival is evidently inhibited, perhaps by low metallicity (Gonzalez 1998; Gonzalez et al. 2001; Santos, Israelian, Mayor 2001), ultraviolet evaporation (Armitage 2000), or collisional disruption (Bonnell et al. 2001) of the proto-planetary disks in this crowded stellar environment.

1.5. Open Clusters

Open cluster surveys should help to clarify the factors that control the formation and survival of planets by characterizing Hot Jupiter populations as functions of age, metallicity and crowding. Wide-field CCD cameras on 1–4 m telescopes with $\sim$ 0.5–1° fields are suitable for surveying 14–22 mag stars in open cluster fields. St.Andrews is involved in a project using the Wide-Field Camera on the UK's 2.5 m Isaac Newton Telescope on La Palma. With 30 bright nights we have monitored $\sim$ 40,000 17–22 mag main-sequence stars in the fields of NGC 6819, 6410, and 7789. With psf-fitting photometry followed by self-calibration of systematic errors in the lightcurves, the rms accuracy approaches $\sim 4\times10^{-3}$mag. The fainter cluster stars have smaller radii, hence deeper transits, making the transit detection sensitivity almost independent of star mass. We are identifying dozens of new variable stars (Street et al. 2002) and will hopefully soon be able to report on candidates for transiting planets.

1.6. Wide-Angle Surveys

Wide angle transit surveys probably offer the most exciting discovery potential. Bright stars (7–14 mag) require small ($\sim$ 10 cm) wide-angle ($5^\circ - 10^\circ$) CCD cameras. The main challenge is to achieve 10^{-3}mag accuracy differential photometry over a very wide field of view, with airmass, transparency, differential refraction, seeing, and even the heliocentric time correction, all varying significantly across the field. A number of surveys are underway:

Table 1. Wide Angle Transit Surveys

name	start	diam (cm)	field of view	pixel (arcsec)	CCD format
Vulcan	1998	8	$7^\circ \times 7^\circ$	6	4k×4k
STARE	1999	10	$6^\circ \times 6^\circ$	10	2k×2k
WASP0	2000	6.3	$9^\circ \times 9^\circ$	15	2k×2k
BEST	2001	20	$3^\circ \times 3^\circ$	6	2k×2k

If the requisite accuracy can be achieved (Borucki et al. 2001), these surveys may discover Hot Jupiters transiting thousands of bright nearby main-sequence G, K, and M stars. Given the modest survey depth ($\sim$ 300 pc), the targets are roughly uniform on the sky, and each magnitude yields 4 times more targets. For a rough estimate, if 7th mag HD 208458 is the brightest, then there may be 4 more down to 8th mag, 16 to 9th, 32 to 10th, ... 4000 to 13th and 16,000 to 14th mag.

How long will these surveys take? A $9^\circ\times9^\circ$ field of view may yield 30 new planets down to 14th mag. An all-sky

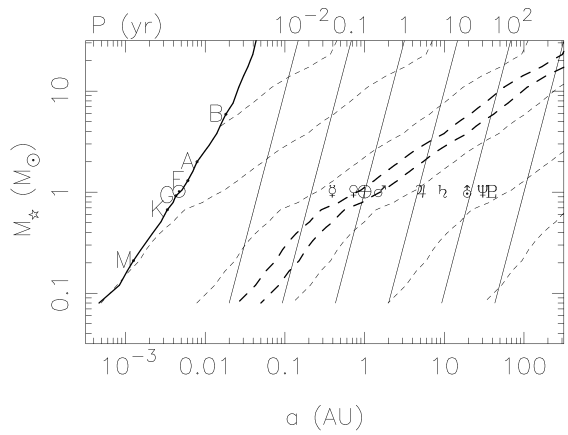

Figure 1. The "habitable zone" is identified here as the region where the equilibrium temperature permits water to exist in liquid form on a rocky planet surface. The temperature declines with distance a from the parent star of star mass M. Stellar radii for different spectral types are shown at the left. The solid and dashed contours give the orbit period P and temperature T at intervals spaced by factors of 10. Solar System planets are marked for reference.

survey of ~ 510 such fields, assuming 2 months per field, would take 85 years with a single camera, and might yield 15 new planets per month. The astronomical community will likely deploy a dozen or more cameras to complete this era of Hot Jupiter discovery in < 7 years.

The resulting catalog of $\sim 10,000$ Hot Jupiters will serve nicely to define their statistics as functions of orbit period, planet size, and star characteristics, to test theories of planet formation and orbit migration. The 100 or so brightest will be suitable for radial velocity and HST follow-up to define the mass-radius relationship of Hot Jupiters as a function of star mass, orbit radius, age, and metallicity. The 10 brightest will yield information on Hot Jupiter atmospheres by direct detection of reflected light (Cameron et al. 1999), revealing albedo spectra, and transmission spectroscopy (transit depth depending on wavelength), revealing absorption spectra (Brown, 2001). This bonanza should be reachable, perhaps in the next 5 years.

1.7. Earth-Like Planets ?

The high accuracy ($\sim 3 \times 10^{-5}$) of *HST*'s lightcurve of HD 209458 suggests that space-borne CCD cameras will be stable enough to detect transits by planets as small as the Earth. *Corot* may find the first, and *Eddington* and *Kepler* are being designed to detect significant numbers of Earth-sized planets in the "habitable zone" around other stars. For lower luminosity stars, the habitable zone moves inward, as shown in Fig. 1.

2. Scaling Laws

We turn now to an analysis leading to scaling laws for the planet catch of a transit search experiment.

2.1. Main Sequence Stars

For our main-sequence star targets, we adopt power-law approximations:

$$R \propto M, \qquad L \propto M^{3.5}, \qquad F \propto M^{4.5} d^{-2} \ , \tag{4}$$

to express the star radius R, luminosity L, and visual flux F in terms of its mass M and distance d. These apply in the range $0.1 < M < 1.7 M_\odot$ (spectral types M8V to F5V). For convenience we take F to be the flux in units of that of the sun viewed from $d = 300$pc, corresponding to $m_V = 12.2$ mag. This turns out to be near the limit of the *Eddington* survey for Earth-analog planets.

2.2. Orbits

For the orbit size we have 3 options: the semi-major axis, a, or (for a given M) the corresponding period P, or temperature T. For a study of Hot Jupiters, P might be the best choice, but since *Eddington* seeks Earth-analog planets, we use T and scale to $T_\oplus \approx 300$ K. The orbit radius and period are then

$$\frac{a}{\mathrm{AU}} = \left(\frac{L}{L_\odot}\right)^{1/2} \left(\frac{T}{T_\oplus}\right)^{-2} \approx \left(\frac{M}{M_\odot}\right)^{7/4} \left(\frac{T}{T_\oplus}\right)^{-2} , \tag{5}$$

$$\frac{P}{\mathrm{yr}} = \left(\frac{a}{\mathrm{AU}}\right)^{3/2} \left(\frac{M}{M_\odot}\right)^{-1/2} \approx \left(\frac{M}{M_\odot}\right)^{17/8} \left(\frac{T}{T_\oplus}\right)^{-3} . \tag{6}$$

We have used Eq.(4) to express a and P in terms of M and T, and will now use these similarly to replace a and P in subsequent expressions.

2.3. Transits

The fractional depth of the transit is

$$\frac{\Delta F}{F} \approx \left(\frac{r}{R}\right)^2 \approx 8.4 \times 10^{-5} \left(\frac{M}{M_\odot}\right)^{-2} \left(\frac{r}{r_\oplus}\right)^2 . \tag{7}$$

The duration of the transit, for $i = 90^\circ$, is

$$\Delta t \approx \frac{2(R+r)P}{2\pi a} \approx 13 \left(\frac{M}{M_\odot}\right)^{11/8} \left(\frac{T}{T_\oplus}\right)^{-1} \ \mathrm{h} . \tag{8}$$

The probability that a randomly-oriented circular orbit exhibits transits is

$$P_t \approx \frac{R+r}{a} \approx 0.005 \left(\frac{M}{M_\odot}\right)^{-3/4} \left(\frac{T}{T_\oplus}\right)^2 . \tag{9}$$

Of course the depth, duration and shape of the transit lightcurve depend on the inclination and limb darkening, but these rough estimates suffice here. We will do better in §3.

2.4. Photometric Accuracy of Lightcurves

The photon flux from Vega ($m_V = 0$) is $\approx 10^3$ cm^{-2}s^{-1}Å^{-1}, for wavelengths near $\lambda \sim 5500$Å. The number of photons from a star of flux F (in units of the 12.2 mag sun at 300 pc) detected in an exposure time Δt is then

$$N_\gamma \approx 10^{10}\ F \ \frac{A}{0.63\,\mathrm{m}^2}\ \frac{Q}{0.7}\ \frac{\Delta\lambda}{4000\text{Å}}\ \frac{\Delta t}{13\ \mathrm{hr}}\quad , \tag{10}$$

where we scale to the *Eddington* baseline design, with pupil area $A \approx 0.63\,\mathrm{m}^2$, detection efficiency (CCD+optics) $Q \approx 0.7$, and bandwidth (unfiltered) $\Delta\lambda \approx 4000$ Å.

Assuming that the dominant source of noise is counting statistics from the star's photons (see §3.1), the accuracy achieved in the lightcurve is

$$\begin{aligned}\frac{\sigma}{F} &= N_\gamma^{-1/2} \\ &\approx 10^{-5}\left(F\ \frac{A}{0.63\,\mathrm{m}^2}\ \frac{Q}{0.7}\ \frac{\Delta\lambda}{4000\text{Å}}\ \frac{\Delta t}{13\ \mathrm{hr}}\right)^{-1/2}\quad .\end{aligned} \tag{11}$$

2.5. Transit Detection

The signal-to-noise ratio, S_1, for detecting a single transit is

$$\begin{aligned}S_1 &= \frac{\Delta F}{\sigma} \approx 8\left(\frac{A}{0.63\,\mathrm{m}^2}\ \frac{Q}{0.7}\ \frac{\Delta\lambda}{4000\text{Å}}\right)^{1/2} \\ &\times\left(\frac{d}{300\ \mathrm{pc}}\right)^{-1}\left(\frac{M}{M_\odot}\right)^{15/16}\left(\frac{r}{r_\oplus}\right)^{2}\left(\frac{T}{T_\oplus}\right)^{-1/2}\quad .\end{aligned} \tag{12}$$

We have set the exposure time equal to the transit duration Δt from Eqn.(8), and substituted for ΔF from Eqn.(7), for σ from Eqn.(11), and for F from Eqn.(4). The first line collects factors characterizing the experiment, followed by those concerning the star and planet.

If we now observe continuously for a time t, a planet with orbit period P will exhibit a number of transits

$$N_t = \frac{t}{P} = \left(\frac{t}{\mathrm{yr}}\right)\left(\frac{M}{M_\odot}\right)^{-17/8}\left(\frac{T}{T_\oplus}\right)^{3}\quad . \tag{13}$$

Phase-folding on the orbit period superimposes the N_t transits, increasing the signal-to-noise ratio for transit detection from S_1 to

$$\begin{aligned}S_N &= S_1 N_t^{1/2} \approx 8\left(\frac{A}{0.63\,\mathrm{m}^2}\ \frac{Q}{0.7}\ \frac{\Delta\lambda}{4000\text{Å}}\ \frac{t}{\mathrm{yr}}\right)^{1/2} \\ &\times\left(\frac{M}{M_\odot}\right)^{-1/8}\left(\frac{r}{r_\oplus}\right)^{2}\left(\frac{T}{T_\oplus}\right)\left(\frac{d}{300\ \mathrm{pc}}\right)^{-1}\quad .\end{aligned} \tag{14}$$

Notice that the dependence on M almost cancels. The fainter lower-mass stars have noisier lightcurves, but their transits are deeper and more frequent, rendering the detection sensitivity, for fixed T and d, almost independent of M.

2.6. Survey Distance and Volume

The maximum distance d to which a transit can be detected with signal-to-noise ratio S, obtained by rearranging Eqn.(14), is

$$\begin{aligned}d &= 300\ \mathrm{pc}\left(\frac{S}{8}\right)^{-1}\left(\frac{A}{0.63\,\mathrm{m}^2}\ \frac{Q}{0.7}\ \frac{\Delta\lambda}{4000\text{Å}}\ \frac{t}{\mathrm{yr}}\right)^{1/2} \\ &\times\left(\frac{M}{M_\odot}\right)^{-1/8}\left(\frac{r}{r_\oplus}\right)^{2}\left(\frac{T}{T_\oplus}\right)\quad .\end{aligned} \tag{15}$$

The survey distance increases rapidly as r^2T for larger and hotter planets, but depends on star mass only weakly, as $M^{-1/8}$.

The volume of a survey covering solid angle Ω ($\Omega = 7.^\circ4^2$ for *Eddington*) and extending to distance d, is

$$\begin{aligned}\frac{\Omega d^3}{3} &\approx 2\times 10^4\mathrm{pc}^3 \\ &\times\frac{\Omega}{7.^\circ4^2}\left(\frac{S}{8}\right)^{-3}\left(\frac{A}{0.63\,\mathrm{m}^2}\ \frac{Q}{0.7}\ \frac{\Delta\lambda}{4000\text{Å}}\ \frac{t}{\mathrm{yr}}\right)^{3/2} \\ &\times\left(\frac{M}{M_\odot}\right)^{-3/8}\left(\frac{r}{r_\oplus}\right)^{6}\left(\frac{T}{T_\oplus}\right)^{3}\quad .\end{aligned} \tag{16}$$

2.7. Number of Stars and Planets

A uniform density of stars is a reasonable approximation if the survey volume is not too deep and remains inside the Galactic disk. If we look at $b = 90^\circ$, perpendicular to the disk, the density of stars may be modeled as decreasing exponentially with a scale height H. A deep survey extending to $d \gtrsim \ell$, where $\ell = H/\sin b$ is the effective scale height along the line of sight at latitude b, looks outside the disk, reducing its effective volume to $\approx \Omega\ell^3/3$.

For the F, G, K, and M stars of interest, Galactic disk scale heights increase with M and are comparable to the 300 pc distance. Over such distances, neglect of extinction by interstellar dust (~ 1 mag kpc^{-1}) is not a major error, especially if a field with relatively low extinction is chosen. Star counts presented in §3.3. suggest a factor $\lesssim 2$ difference between the Galactic plane and pole.

For rough estimates, we assume a uniform density of stars, and adopt a power-law stellar mass function

$$\frac{dn_\star}{dM} \approx \frac{0.1}{\mathrm{pc}^3 M_\odot}\left(\frac{M}{M_\odot}\right)^{-B}\quad , \tag{17}$$

where the slope is $B \approx 2.35$ for a Salpeter mass function.

To find the number of planets detected, N_p, we count the stars inside the survey volume that exhibit transits by planets of the type we seek. Each star is weighted by the planet function, $f(r, T|M)$, which gives the number of planets with radii from r to $r + dr$ and temperature T to $T + dT$ for stars of mass M. To omit stars with incorrect orbit orientations, we weight the stars by transit probability $P_t(M,T) \propto M^{-3/4}T^2$ from Eq.(9). Putting all this together, the planet catch is

$$\begin{aligned} N_p &= \frac{\Omega d^3}{3} \int dM \frac{dn_\star}{dM} \int\int dr\ dT\ P_t(M,T)\ f(r,T|M) \\ &\approx 10^2\ \frac{\Omega}{7^\circ 4^2} \left(\frac{S}{8}\right)^{-3} \left(\frac{t}{\text{yr}}\ \frac{A}{0.63\,\text{m}^2}\ \frac{Q}{0.7}\ \frac{\Delta\lambda}{4000\text{Å}}\right)^{3/2} \\ &\times \int \frac{n_\star}{0.1\text{pc}^{-3}} \frac{dM}{M_\odot} \left(\frac{M}{M_\odot}\right)^{(9/8-B)} \\ &\times \int\int dr\ dT \left(\frac{r}{r_\oplus}\right)^6 \left(\frac{T}{T_\oplus}\right)^5 f(r,T|M)\ . \end{aligned} \tag{18}$$

The planet function $f(r,T|M)$, is an unknown distribution over planet type for each star mass. To place f_H Earth-radius planets in the "habitable zone", the temperature range $T_C = 250$K to $T_H = 350$K, we may adopt

$$f(r,T|M) = \frac{f_H\ \delta(r-r_\oplus)}{T \ln\left(T_H/T_C\right)}\ , \qquad \text{for } T_C < T < T_H\ , \tag{19}$$

where $\delta(r)$ is a Dirac δ-function. Evaluating the integrals then suggests $N_p \sim 10 f_H$, With most of the detections arising from low-mass stars, and given the use of power-law approximations, the uncertainty in this estimate is at least a factor ~ 3.

To obtain analytic results we have adopted a uniform star density and various power-law approximations to main-sequence star properties. The Monte-Carlo simulations presented in §3 improve on these assumptions.

2.8. Optimizing a Transit Survey

The value of having scaling laws is to see how the planet detection capabilities depend on parameters which define the experiment (S,Ω, A,Q,$\Delta\lambda$, t), and on the type of star (M) and planet (r, T) being sought. For experiments like *Eddington*, which is limited by star photon counting noise and surveys a volume largely within the thickness of the Galactic disk, the figure-of-merit to maximize planet detection performance is the survey volume from Eq.(16), scaling as

$$\Omega d^3 \propto S^{-3}\Omega\left(A\ Q\ \Delta\lambda\ t\right)^{3/2}\ . \tag{20}$$

If we make use of N identical telescopes, these may be used to multiply Ω by N, if they point at different fields, or to multiply A by N, if they point at the same field. From the perspective of planet detection, the later would appear to be more advantageous choice.

The steep dependence of the planet catch on signal-to-noise threshold S indicates the critical importance of using optimal data analysis techniques. Sloppy work, requiring adoption of a conservative S/N threshold to keep false alarm rates down, will dramatically reduce the number of detected planets.

3. Monte-Carlo Simulations of the Planet Catch

We have developed a Monte-Carlo simulator to evaluate the numbers and types of planets that can be detected in a transit survey. Each run generates a random catalog of the stars and detected planets within the survey volume for each type of star and planet. From one or more such catalogs, the statistical characteristics and correlations among the parameters of the stars and detected planets can be evaluated. Such results may provide useful guidance in the optimization of design parameters for the *Eddington* mission, and other planet transit surveys.

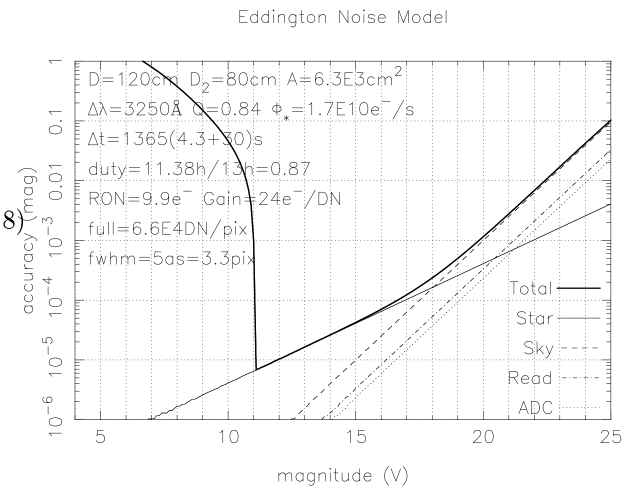

Figure 2. Accuracy of Eddington *photometry for constant stars as function of visual magnitude for a 13-hour exposure consisting of a cycle of 30s exposures with 4.3s readout time.*

We discuss below several aspects of the simulator, illustrating with results for the *Eddington* baseline design. The improvements made here, compared with the rough calculations done in §2, include (1) relaxing the assumption of uniform star density, (2) including extinction by interstellar dust (3) using an empirical stellar mass function, (4) an accurate main sequence star model for $R(M)$, $L(M)$, and $F(\lambda,M)$, (5) an instrumental sensitivity curve $P(\lambda)$, (6) more elaborate CCD noise model, (7) allowing for $i < 90^\circ$ when evaluating the S/N for transit detection.

3.1. CCD Noise Model

Fig. 2 predicts the accuracy of *Eddington* photometry vs the star magnitude m_V for a lightcurve binned to 13-hour time resolution. The calculation assumes that the CCD camera is de-focused to produce Gaussian star images with a 5-arcsecond (3.3 pixel) fwhm. The 13-hour exposure is really a series of 30s exposures separated by 4.3s CCD readouts, accumulating photons for 1365×30s$=11.83$ h, a duty cycle of 0.87. The adopted spectral sensitivity curve, shown in Fig. 3, includes the CCD quantum efficiency and reflection from 3 mirrors. The simple Poisson noise calculation in Eqn. 11, which predicts $\sigma/F \approx 10^{-5}$ at $m_V = 12.2$, is seen to be fairly accurate for $11 \lesssim m_V \lesssim 17$.

For stars fainter than $m_V \sim 17$ mag, the accuracy becomes background noise limited, the background arising from zodiacal dust emission. CCD readout noise is

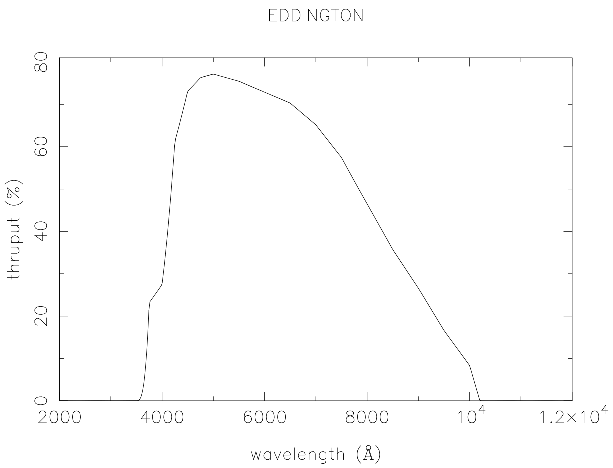

Figure 3. Sensitivity curve of the Eddington *CCD camera including the quantum efficiency curve of the CCD and reflection from 3 mirrors.*

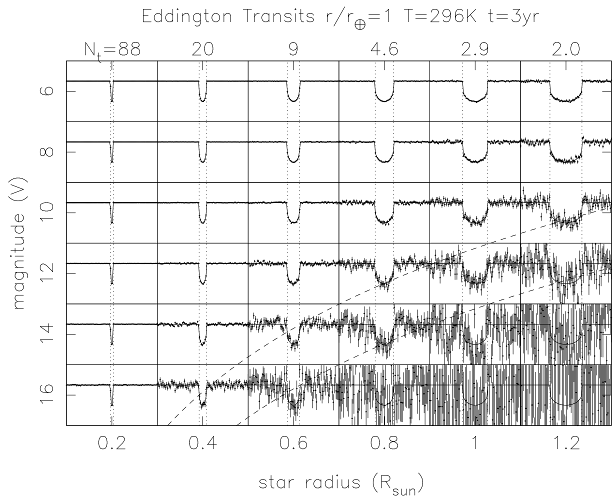

Figure 4. Simulated Eddington *lightcurves of Earth-like planets transiting stars with different V magnitude and radius. The simulation is for a planet with the same radius and temperature as Earth. Each lightcurve shows a 48-hour subset of the* Eddington *data after folding on the planet orbit period and binning to 30-minutes time resolution. The dashed lines show the adopted limiting magnitude for detection S/N thresholds* $S_N = 12$ *and 30.*

included but unimportant. Crowded field effects are not yet included in the simulation, and may be important.

A bright limit at $m_V \sim 11$ mag is set by CCD saturation. Shorter exposures or further de-focusing can improve the saturation limit. De-focusing the star images increases crowding and sky noise, while shorter exposures diminishes the duty cycle.

In the present simulations, we neglect systematic errors (e.g. due to image motion, focus changes, errors in the CCD flat field) and intrinsic stellar variability on the relevant timescale. For space-based surveys the stable point-spread function and accurate tracking to keep star images stationary to a small fraction of a CCD pixel will help to keep flat-fielding problems within bounds.

3.2. Simulated Transit Lightcurves

Fig. 4 shows a set of simulated *Eddington* lightcurves for Earth analogs ($T = T_\oplus$, $r = r_\oplus$) transiting stars of different R and m_V. Dashed lines calculated from Eqn. (14) for $S_N = 12$ and $S_N = 30$ appear to give a good representation of the limiting magnitude. The estimate that an Earth-analog system can be detected down to 12-13 mag is confirmed.

3.3. Star Counts

For the simulator, we assume that the space density of main-sequence stars falls off exponentially with height above the Galactic plane. For stars of mass M, the density of stars on the plane $dn_\star(M)/dM$, and the scale height $H(M)$, are interpolated from Table 2 in Robin & Creze (1986). The number of stars brighter than apparent magnitude m_V is

$$N_\star(< m_V) = \int\int\int d^2\Omega \; dM \; \frac{dn_\star}{dM} \int_0^d e^{-x/\ell} x^2 \; dx \; . \quad (21)$$

Here Ω is the solid angle of the survey, x is distance along the line of sight, $\ell(M,b) = H(M)/\sin b$ is the effective scale length along the line of sight, b is Galactic latitude, $H(M)$ is the exponential scale height for stars of mass M, $d(M, m_V)$ is the distance at which a star of mass M has apparent magnitude m_V.

The resulting cumulative star counts vs apparent magnitude and spectral type for galactic latitudes $b = 90°$ and $10°$ are shown in Fig. 5 for the *Eddington* field of view. A constant density approximation, giving 4 times more stars for each magnitude of depth, and little dependence on Galactic latitude b, is accurate for the F, G, K, and M stars of interest down to 10, 13, 15, and 18 mag respectively. The star count converges as we reach fainter stars with distances extending outside the Galactic disk. On each line of sight the mean spectral type of the stars becomes later as we go fainter.

At low galactic latitudes the background of distant O, B, and A stars outnumber the G, K, and M targets for $m_V \lesssim 15$ mag. For $b = 90°$, such background stars are absent. The issue of crowding by background stars needs to be considered carefully. It is not immediately obvious that it is better to point at the Galactic plane.

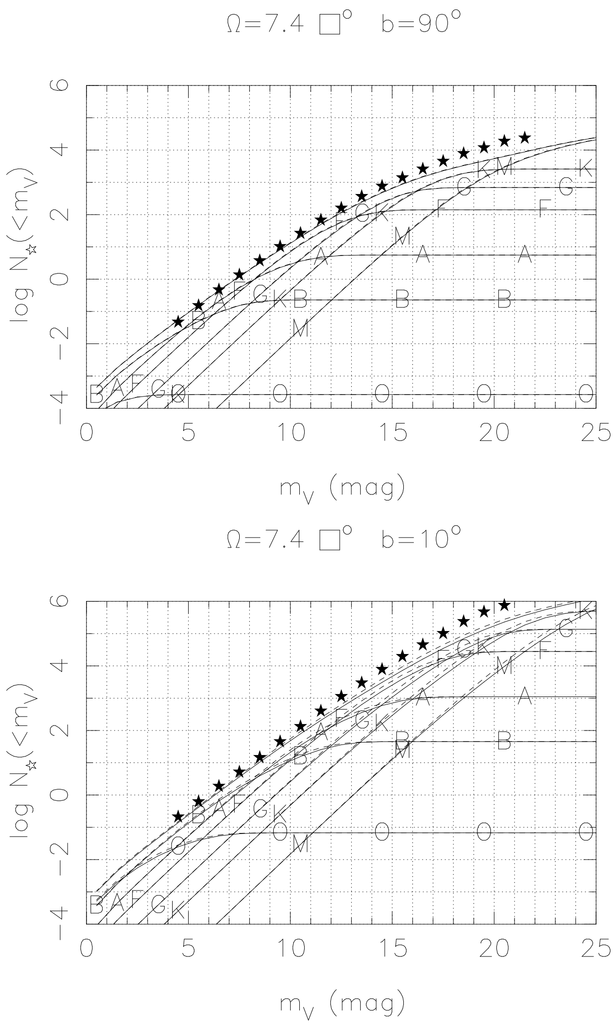

Figure 5. Cumulative star counts in the Eddington *field of view for main sequence stars of spectral types O,B,A,F,G,K,M for Galactic latitudes $b = 10°$ and $90°$. The model is validated by comparison with observed total star counts (stars). Dashed curves omit extinction by interstellar dust, showing that this has little effect.*

3.4. The Planet Catch

The number of planets detected is

$$N_p = \int\int\int d^2\Omega \; dM \; \frac{dn_\star}{dM} \times \int\int dr \; dT \; P_t(M,T) \; f(r,T|M) \times \int_{d_1(M)}^{d_2(r,T,M)} e^{-x/\ell} \; x^2 \; dx \; . \tag{22}$$

We now integrate over many lines of sight through the survey volume. The distance limits are $d_1(M)$, where stars of mass M saturate the CCD exposures, to $d_2(r,T,M)$, beyond which transits are no longer detectable. Inserting habitable Earths using the planet function $f(r,T|M)$ from Eq.(19), we again find $\sim 10 f_H$ Earth-analog planets.

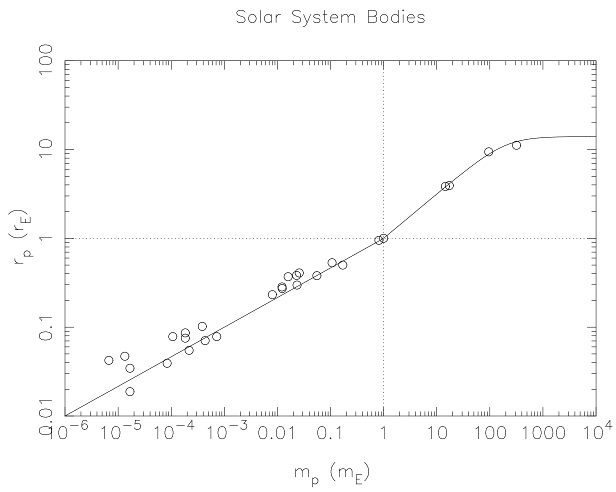

Figure 6. Mass-radius relationship for Solar System bodies including planets, moons, and asteroids.

3.5. Planet Functions

The planet catch clearly depends not only on the transit detection capabilities of the experiment, and the number of stars inside the survey volume for each star and planet type, but also on the *planet function*, $f(r,T|M)$, which gives the number of planets per star, as a distribution over planet size r and temperature T, and as a function of star mass M.

At present we have little hard information about the planet function. We know the pattern of planets in our solar system, and the distribution of Doppler wobble planets. It is a long extrapolation from Hot Jupiters to Habitable Earths. There is a correspondingly large uncertainty in predicting the number of Habitable Earths that *Eddington* may detect. A primary scientific goal of *Eddington*, and other planet search experiments, is to fill in this missing information on the numbers of large and small planets at different temperatures around large and small stars. This will help in developing and testing theories for the formation, survival, and evolution of these worlds.

By looking at a couple of different planet functions, we can get a feel for this uncertainty, and the corresponding leverage that *Eddington* will have to measure the planet function. Start by assuming that all stars have 9 planets with the same r and T as for the 9 solar planets. How many of these solar systems will *Eddington* detect?

Table 2. Number of Detected Solar Systems

	M	V	E	M	J	S	U	N	P
$b = 10°$	0	7	5	0	230	50	1	0	0
$b = 90°$	0	7	5	0	33	12	1	0	0

The total number of planets found is not large, because our solar system is lacking in close-in planets. The number of times Jupiter and Saturn are detected depends strongly on b, while the numbers for smaller planets do not. This is because the deeper transits caused by gas giants are detectable to much greater distances, while the smaller planets can be found only on nearby stars.

Now consider a power-law planet function,

$$f(a,m|M) \propto a^{\alpha} m^{\beta} M^{\gamma} \ . \tag{23}$$

We spread the planets with power-law distributions over $0.03 < a < 100$ AU, $0.5 < m < 3000\ m_{\oplus}$, $0.08 < M < 10\ M_{\odot}$. This specifies the planet *mass* distribution, and we obtain *radii* from the mass-radius relationship that is shown in Fig.6 along with the masses and radii of Solar System planets, moons, and asteroids.

We adopt $\gamma = 0$, making the planet function independent of star mass. For $\gamma = 1$, the total mass in planets would scale with M. We currently lack information on this, because the Doppler wobble surveys have not yet targeted a wide range of star masses.

The Doppler wobble planets are roughly uniform in $\log a$ and $\log m$, suggesting $\alpha = -1$, $\beta = -1$. Bode's law in the Solar System is also roughly compatible with $\alpha = -1$. We adopt $\alpha = -1$, and consider two cases $\beta = -1, -1.5$. We also impose a period cutoff at $P <$ 3d.

To compare the planet functions, Table 3 shows the number of planets per star for 4 categories: "Jupiters", with $r > R_J$, "Hot Jupiters", with $r > R_J$ and $P = 3-5$ d, "Earths", with $r > R_{\oplus}$, and "Water" worlds, with $r > R_{\oplus}$ and $T = 250 - 350$ K. We normalize to 0.01 Hot Jupiters per star, thus roughly matching the result found for Doppler wobble planets. The m^{-1} case has far fewer small planets, and the $m^{-1.5}$ case has more small planets than the solar system.

Table 3. Comparison of Planet Functions

$f(a,m)$	Hot Jups 3–5 d	Jupiters $r > R_J$	Earths $r > R_{\oplus}$	Water 250–350 K
$a^{-1}m^{-1}$	0.01	0.24	0.85	0.07
$a^{-1}m^{-1.5}$	0.01	0.25	6.55	0.54
solar r, T	0	1	5	1

3.6. Monte-Carlo Catalogs

The catalog of 13,000 (!) detected planets from the Monte Carlo simulation for $f \propto a^{-1}m^{-1.5}$, and $b = 10°$ is shown in Fig. 7. The planets are projected onto various pairs of axes to show the types of stars and planets found. The vast majority are large hot planets, with only a handful fallling in the "Habitable Earth" region on the $r - T$ projection. Results for $f \propto a^{-1}m^{-1}$ are similar but with far fewer low-mass planets. The number of Hot Jupiters is well anchored from Doppler wobble planets, but the extrapolation to lower masses is quite uncertain.

4. Summary

After reviewing the present status and bright prospects for discovery of 1000 Hot Jupiters in ground-based transit search programmes, we derived scaling laws and described Monte-Carlo simulations that are being using to evaluate

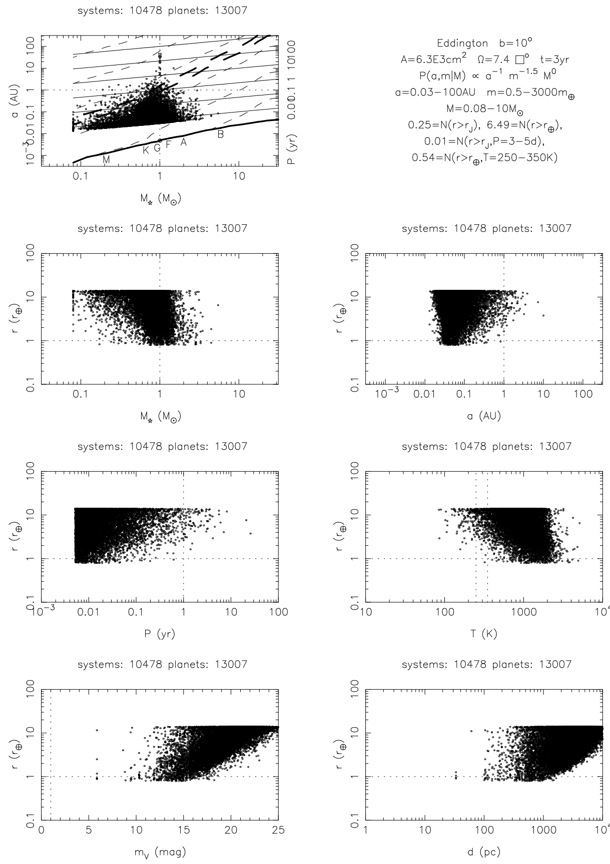

Figure 7. The planet catch for a Eddington *field of view for a 3-year mission at Galactic latitude $b = 10°$.*

planet detection capabilities of *Eddington* and other transit survey experiments.

The scaling laws employ power-law approximations to the properties of main-sequence stars in order to obtain analytic expressions for the planet catch in terms of parameters that define the experiment and the types of stars and planets.

For planets of fixed T and r, on stars of mass M, the survey distance scales as $d \propto M^{-1/8} r^2 T$. The survey volume scales as $T^3 r^6$, and the planet count scales as $T^5 r^6$. Large hot planets are strongly favoured. *Eddington* should detect thousands of "Hot Jupiters" with 3-5 day periods, with some certainty since Doppler wobble studies establish their presence around $\sim 1\%$ of nearby sun-like stars. *Eddington* should also find dozens of "hot Earths", if they exist, with larger uncertainties because the mass function of small planets is not yet known.

Our results indicate that the baseline design for *Eddington* will deliver a handful of "habitable Earths", if they exist in significant numbers. If performance falls a bit short of the somewhat idealized assumptions made in our simulations, then *Eddington* may tell us little about habitable Earths. Studies are therefore underway to identify design changes that can significantly enhance the planet detection capabilities.

If we wish to detect transits with S/N ratio S, using a telescope with effective area A and bandwidth $\Delta\lambda$ to cover a solid angle Ω for a time t, the survey volume we probe scales as

$$\Omega d^3 \propto S^{-3}\Omega(A\ \Delta\lambda\ t)^{3/2}\ . \tag{24}$$

This is an appropriate figure of merit against which to judge options and optimize parameters of transit survey experiments. The strong dependence on S means that optimal data analysis methods are critical to success.

Once a field is selected, the same methods outlined here, but using the actual numbers of main sequence stars of different types and distances, can be used to evaluate the likely planet catch.

Acknowledgements

Keith Horne thanks PPARC for a Sr. Fellowship and The University of Texas Austin for a Beatrice Tinsley Visiting Professorship which made this work possible.

References

Armitage, P.J. 2000, A&A 362, 968.

Bonnell, I.A., Smith, K.W. Davies, M.B., Horne, K. 2001, MNRAS 322, 859.

Borucki, W.J., et al. 2001, PASP 113, 439.

Brown, T.M., 2001, ApJ 553, 1006.

Brown, T.M., Charbonneau, D., Gilliland, R.L., Noyes, R.W., Burrows, A. 2001, ApJ 552, 699.

Cameron, A.C., Horne, K. Penny, A., James, D. 1999, Nature 402, 751.

Charbonneau, D., Brown, T.M., Latham,D.W., Mayor,M. 2000, ApJ 529, L45.

Gilliland, R.L., et al. 2000, ApJ 545, L47.

Gonzalez, G. 1998, A&A 334, 221.

Gonzalez, G. Laws, C., Tyagi, S., Reddy, B.E. 2001, AJ 121, 432.

Henry, G.W., Marcy, G.W., Butler, R.P., Vogt, S.S. 2000, ApJ 529, L41.

Jha, S., Charbonneau, D., Garnavich, P.M., Sullivan, D.J., Sullivan, T., Brown, T.M., Tonry, J.L. 2000, ApJ 540, L45.

Mayor, M., Queloz, D. 1995, Nature 378, 355.

Robin, A.C., Creze, M. 1986, A&A 157, 71.

Santos, N.C., Israelian, G., Mayor, M. 2001, A&A 373, 1019.

Street, R.A., et al. 2002, MNRAS, in press.